Computed Tomography Image Origin Identification based on Original Sensor Pattern Noise and 3D Image Reconstruction Algorithm Footprints

Yuping Duan, Dalel Bouslimi, *Member, IEEE,*
Guanyu Yang, and Huazhong Shu, *Senior Member, IEEE,* Gouenou Coatrieux, *Senior Member, IEEE*

***Abstract*—In this paper, we focus on the "blind" identification of the Computed Tomography (CT) scanner that has produced a CT image. To do so, we propose a set of noise features derived from the image chain acquisition and which can be used as CT-Scanner footprint. Basically, we propose two approaches. The first one aims at identifying a CT-Scanner based on an Original Sensor Pattern Noise (OSPN) that is intrinsic to the X-ray detectors. The second one identifies an acquisition system based on the way this noise is modified by its 3D image reconstruction algorithm. As these reconstruction algorithms are manufacturer dependent and kept secret, our features are used as input to train an SVM based classifier so as to discriminate acquisition systems. Experiments conducted on images issued from 15 different CT-Scanner models of 4 distinct manufacturers demonstrate that our system identifies the origin of one CT image with a detection rate of at least 94% and that it achieves better performance than Sensor Pattern Noise (SPN) based strategy proposed for general public camera devices.**

***Index Terms*—Image origin identification, Computed Tomography, Sensor Pattern Noise, 3D Image reconstruction algorithm.**

I. Introduction

THE rapid development of internet and digital technologies brings increasingly more digital medical data to patient cares. That is the case of medical images that are produced by various medical imaging apparatus and shared in a wide variety of applications ranging from daily medical practice to telediagnosis up to telesurgery [1]. If image distribution and manipulation are easier, security issues in terms of confidentiality, availability, reliability and traceability are also increased [2]. In this paper, we focus on the particular problem of Computed Tomography (CT) image origin identification, that is to say being able to show a CT image has been produced by a specific CT-Scanner system. Even though the standard for medical image storage and transfer, DICOM (Digital Imaging and Communications in Medicine - medical.nema.org), traces image modifications and transmissions by means of "indicators" in the image file header [3], these indicators are prone to manipulation and information loss. Such a modification can easily be conducted with the help of medical image software freely available [4]. As a consequence, one may doubt about the real image origin.

To overcome this issue, one can digitally sign an image [5] or watermark it with a proof of its origin [6]. In digital signature based schemes, a hash of the image is captured and asymmetrically encrypted for non-repudiation purpose [7] and transmitted along with the image. At the reception, if the attached signature does not match the recomputed one, the image integrity and origin are not correct. Watermarking based verification techniques consist in embedding into the image an identifier of the modality which issued it [2]. If the embedded message is not valid or retrieved, an alarm will be raised [8]. To be efficient, these hashing or watermarking schemes need to be implemented inside the image acquisition device [9, 10]. This may limit their use in real practice.

To go further, a question is how to verify the origin of a given CT image, i.e., identifying the model/brand of the CT-Scanner system that issued it, only from its pixels' gray values. To answer this question one can take advantage of digital forensics approaches which focus on origin identification, integrity verification and authentication of data [11]. Most of these techniques have been proposed in the case of general public devices (e.g. cameras, optical scanners or mobile phones) [12]. They can be distinguished into two classes. Methods of the first class analyze the image acquisition chain in order to identify characteristics that are specific and unique to it. As example, processes such as Color Filter Array (CFA) interpolation [13],

This work was supported by the National Natural Science Foundation of China under Grants 61271312, 61201344, 61401085, 31571001, and 81530060, and by Natural Science Foundation of Jiangsu Province under Grant BK2012329, BK2012743, DZXX-031, BY2014127-11, by the '333' project under Grant BRA2015288 and by the Qing Lan Project.

Y. Duan is with the LIST Southeast University, Nanjing, China; Institut Mines-Telecom, Telecom Bretagne; INSERM U1101 LaTIM, 29238 Brest Cedex, France (e-mail: duanyp11@gmail.com).

D. Bouslimi and G. Coatrieux are with the Institut Mines-Telecom, Telecom Bretagne; INSERM U1101 LaTIM, 29238 Brest, France (e-mail: gouenou.coatrieux@telecom-bretagne.eu;dalel.bouslimi@telecom-bretagne.eu).

G.Y. Yang and H.Z. Shu are with the Laboratory of Image Science and Technology, School of Computer Science and Engineering, Southeast University, Key Laboratory of Computer Network and Information Integration (Southeast University), Ministry of Education, 210096 Nanjing China, and also with Centre de Recherche en Information Biomédicale sino-français, 210096 Nanjing China (e-mail: yang.list@seu.edu.cn; shu.list@seu.edu.cn).

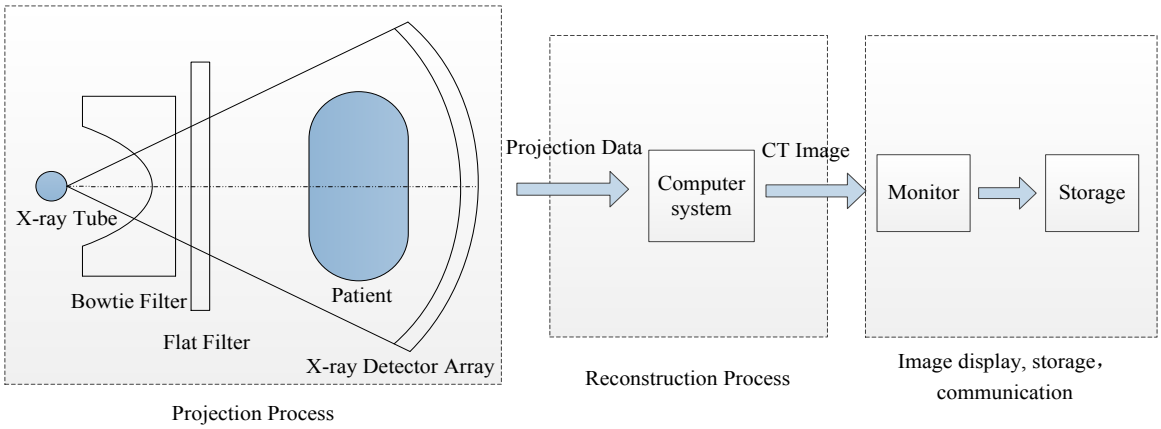

Fig. 1. Basic principles of a CT-Scanner system.

demosaicing algorithms [14], white balancing algorithms [15] or JPEG compression [16] leave specific signal distortions that can be used for device identification. Some other works explore classifier-based strategies to put in evidence statistical image footprint. Finding suitable image features is the key point of these approaches. Some of them correspond to color features, image quality features and image characteristics in the frequency domain [17-19]. One problem of such a technique is that manufacturers usually make use of the same processes in their different device models. That is especially the case of general public devices making hard to identify a device uniquely.

Regarding the second class of methods, the interest is given to physical phenomena that are inherent to the acquisition chain components and which can be used as device footprint if correctly captured. This is the case, for example, of lens distortions [20] and sensor imperfections [21]. In [22], in the case of raw images (i.e., non lossy compressed image), Thai *et al.* established a two parameter noise model with the likelihood ratio test (LRT) that clearly differentiates the camera that has acquired an image. Lukas *et al.* were the first to introduce a forensic technology based on Sensor Pattern Noise (SPN) [23]. SPN is defined as any noise component that is intrinsic to sensor and cannot be eliminated by averaging. Due to sensor manufacturing imperfections, pixel values vary from a sensor to another under the same illumination. The photo response non-uniformity noise (PRNU) is the main SPN component. It is generated by the camera Charge Coupled Device (CCD) and can serve as unique camera footprint [24]. PRNU based identification consists in computing the PRNU footprint of a device and detecting it into an image by means of correlation measurements. Obviously, the efficiency of these methods is dependent upon the ability to reliably extract such noise from images. To our knowledge, only two works have focused on medical image origin identification. In [25], Duan *et al.* demonstrated the existence of a Digital Radiography Pattern Noise (DRPN) footprint for digital radiography images. Kharboutly *et al.* experimentally expanded this approach to CT-Scanner [26]. The footprint they proposed is computed from one CT volume. It corresponds to the average of SPNs extracted from each volume slice.

In this work, we explore a novel approach which takes advantage of the principle of CT-Scanner acquisition system. We suggest extracting the Original Sensor Pattern Noise (OSPN) from a CT image by inverting back the 3D image reconstruction process. Based on this OSPN we show it is already possible to identify the CT-Scanner that has issued an image with good accuracy and better performance than with SPN based strategies proposed for general public devices. Then, we propose a set of features which allow distinguishing a CT-Scanner depending on its 3D image reconstruction algorithm. As these algorithms are manufacturer dependent and kept secret, we use these features as input of a classifier we train so as to differentiate CT-Scanners. We further show that the combination of these two approaches leads to better origin identification performance.

The rest of this paper is organized as follows. In Section II, we recall the basic principles of CT-Scanners and the main noise components that are inherent to CT images. We also briefly introduce the most common 3D image reconstruction algorithms. Our OSPN and 3D image reconstruction algorithm footprints are presented in Section III. Experimental results conducted on images issued from 15 different CT-Scanner models of 4 distinct manufacturers, while considering various anatomical objects, are provided and analyzed in Section IV. Conclusions are drawn in Section V.

II. CT-Scanner Noise and Principles of CT 3D Image Reconstruction

A. Basic Principles of CT-Scanner System

The basic principles of X-ray CT-Scanners have not changed from the early days [27, 28]. As schematically depicted in Fig. 1, they consist of a fan-beam X-ray source and a detector array rotating around the patient. CT-Scanner systems make use of these X-ray projections taken from different directions to produce cross-sectional anatomy image of specific areas in a patient's body. The formation of the CT image involves therefore two steps: the projection process and the reconstruction process. A CT-Scanner system starts by a projection process where, while going around a single axis of

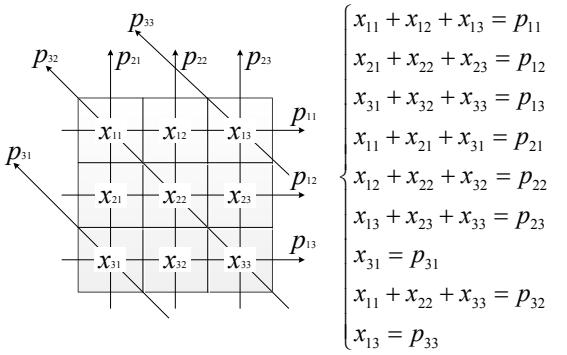

Fig. 2. Illustration of CT 3D image reconstruction. p_{ij} and x_{nm} are projection and pixel values, respectively.

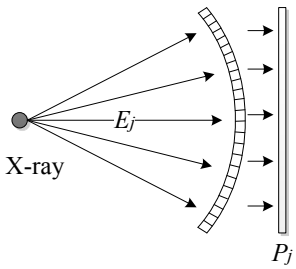

Fig. 3. Generation of projection data.

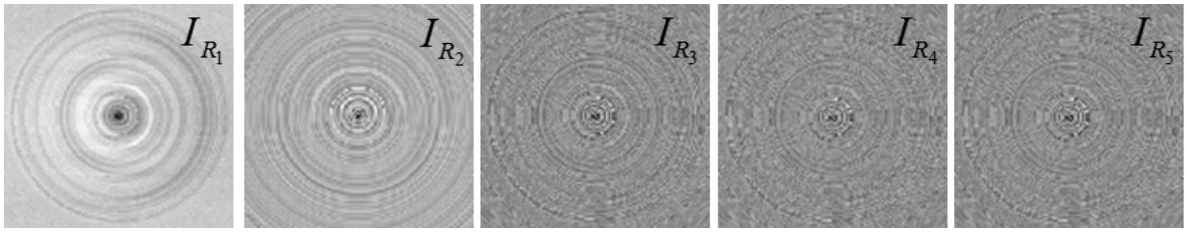

Fig. 4. Slice of 3D image volume having as input the same Gaussian noise. They result from basic 3D image reconstruction algorithms: R_1 - simple back projection; R_2 - inverse radon transformation; R_3 - filtered back projection; R_4 - 2D Fourier transformation; R_5 - back projection using 1D Fourier transformations and central slice theorem.

rotation, X-Rays are emitted and read out by an X-Ray detector array after having passed through two distinct filters and the patient. These radiographic projection data, acquired from different rotation angles (notice that several hundreds of views are used), are then provided to a tomographic reconstruction algorithm in order to build the final CT tomographic image volume that can be next displayed on a monitor for diagnosis, stored and communicated. The basic principle of this reconstruction process is illustrated in Fig. 2, where each projection sample in a view can be seen as the sum of a particular group of pixels' values in the CT image along one direction. The objective is to find the pixel values by solving a system of linear equations, one per angle. Although simplistic, we invite the reader to keep in mind this 3D image reconstruction algorithm illustration, as in the sequel this process will have to be inverted in order to extract the inherent noise of the X-Ray Detector array from the image.

Beyond this simple back projection technique, many improvements in hardware technologies, system design as well as in reconstruction algorithms have been brought over the past two decades. If the fan-beam axial Filtered Back Projection algorithm (FBP - where projection data are filtered before being back projected for image quality improvement) was the major mode of reconstruction for a long time, the helical or spiral CT using a detector array with up to 256 rows (i.e. multislice CT) forces the design of new reconstruction algorithms based on cone-beam geometry. All these advances lead to faster isotropic volume acquisition, higher spatial resolution and better image quality. In parallel, with the progress in computer resources, iterative reconstruction methods now challenge the FBP approach as advocated in [29, 30] due to their ability to incorporate models of the physical process or other prior information. Nevertheless, much more still remain to be done when considering the inherent polychromatic nature of the energy spectrum of X-Ray tubes, the non-linear effects such as scatter or beam hardening, the statistical fluctuations of X-Ray flux on each projection sample over a short sampling duration (less than a millisecond on recent scanners) to which the electronic noise must be added. Notice that each CT-Scanner manufacturer develops its own tomographic reconstruction algorithms. As exposed above, each CT-Scanner model has its own reconstruction algorithm. These algorithms are kept secret as they are important elements of the system added value.

B. CT-Scanner Pattern Noise Modeling

Modelling the noise distributions in the projections is not straightforward because the CT projection raw data undergo manufacturer-specific pre-processing and calibration processes before its use in the reconstruction. This noise is further modified by the 3D image reconstruction process. Given the limited scope and the focus of this paper, we have retained the noise model proposed in [25] for DR systems

$$P_j = E_j + K \cdot E_j + Q \tag{1}$$

where P_j corresponds to the projection data at the angle j; E_j is the "X-Ray" entered into the system (see Fig. 3); $K \cdot E_j$ denotes the Gaussian noise inherent to the X-Ray detector array in the j^{th} projection (a 1D vector in the sequel); Q is the sum of other residual noises. K is the Original Sensor Pattern Noise factor we are interested in. We will estimate it through the noise terms $K \cdot E_j$ in different projections.

The choice of this model was also guided by the fact that although the major manufacturers are using similar analytical or iterative reconstruction methods, they remain black boxes.

Sufficient information on the underlying algorithms and implementation is missing and most system parameters are unknown. Nevertheless, and as we will see, it is possible to discriminate the origin of one CT image by using the model in (1) and by training some classifiers.

III. CT-Scanner Identification

In this section, we describe how to calculate the footprints we propose in order to identify the CT-Scanner that has issued an image using the Original Sensor Pattern Noise and a set of standard CT-Scanner 3D image reconstruction algorithms.

A. CT-Scanner Identification based on OSPN Extraction

As discussed in Section II, we first aim at extracting the OSPN of an image. In order to give the reader an idea of what looks like the original noise into the reconstructed image, we generate a Gaussian noise n to simulate the noise term $K \cdot E_j$ in (1). In the following simulation n is constituted of 512 samples due to the fact that one row of most common X-Ray detector array is constituted of 512 elements. We have then applied 5 different reconstruction algorithms R_i, $i = 1, \ldots, 5$, having as input these noisy projection data with views acquired every 1 degree angle from 1 to 180 degree, that is to say:

$$I_{Ri} = R_i(P_j, j = 1, \cdots \tag{2}$$

where $P_j = K \cdot E_j + n$, $j = 1, 2, \ldots, 180$, I_{Ri} is the image of 512×512 pixels obtained with the analytical reconstruction algorithm R_i. The five algorithms we considered are: R_1- simple back projection; R_2- inverse radon transformation; R_3- filtered back projection; R_4- 2D Fourier transformation; R_5- back projection using 1D Fourier transformations and central slice theorem. The reader interested in these reconstruction techniques may find the essence of the above algorithms in [27, 28].

We give in Fig. 4 some image samples we obtained with the same Gaussian noise n as input, that is to say considering only as input the noise inherent to the X-Ray detector array. We recall that this noise is unique to a sensor and that it consequently exists in all projections (see section II. B). One can see that the reconstructed noise depends on the original sensor noise and also on the reconstruction algorithm.

The strategy we follow in order to get the OSPN of one real CT image is illustrated in Fig. 5, considering 180 acquisition angles only. Its different steps are:

1) Extraction of the CT image noise by means of image filtering. This noise corresponds to the difference between the original CT image Y and its denoised version $F(Y)$:

$$N = Y - F(Y) \tag{3}$$

Note that N is the image noise. In our implementation, $F(\cdot)$ is a wavelet based filter as proposed in [26] for CT image origin identification so as to conduct a fair comparison performance in section IV. As an aside, notice that N is considered as the image SPN in [26], it is a 2D matrix of same dimension as that of the image.

2) Estimation of the projection noise O_j, $j = 1, 2, \ldots, 180$, from the noise image N. O_j is an estimator of the noise term $K \cdot E_j$ in (1). This task is conducted by inverting the back projection algorithm process (i.e. direct projection of image voxels onto the detector row – see Section II.A). By doing so, O_j is a 1D vector of 1×512 samples.

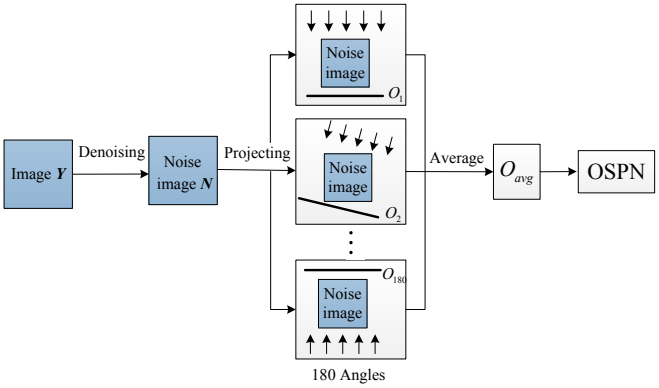

Fig. 5. Image OSPN extraction.

3) Calculation of the average angle noise O_{avg}

$$O_{avg} = \frac{1}{180} \sum_{j=1}^{180} O_j \tag{4}$$

By doing such an average, we expect to enhance the fixed component of the sensor pattern noise. In the sequel O_{avg} corresponds to the image OSPN.

From this standpoint, the identification of one CT image origin simply consists in extracting its OSPN following the above steps and comparing it with the *a priori* known OSPN of a given CT-Scanner. This comparison is established by means of correlation measure ρ:

$$\rho = corr(O, O_{avg}) = \frac{\mathrm{cov}(O, O_{avg})}{\sigma_O \cdot \sigma_{O_{avg}}} \tag{5}$$

where O is the OSPN of one CT-Scanner, we identify as "reference OSPN" in the sequel, and O_{avg} the OSPN extracted from the CT image under observation, $\mathrm{cov}(\cdot)$ is the covariance operator, σ_O and $\sigma_{O_{avg}}$ are the standard deviations of O and O_{avg}, respectively. This correlation ρ is used as a measure of the similarity to classify the CT-Scanners. An experimental threshold can also be determined, in which case, the tested OSPN corresponds to the reference OSPN of a scanner. The scanner the reference OSPN of which gives a correlation value higher than the threshold is chosen as the origin CT-Scanner [25].

B. 3D Image Reconstruction Algorithm Identification

Herein, our basic objective is to identify the image reconstruction algorithm used by a CT-Scanner. Let us come back to our previous CT reconstruction simulation framework. As shown in Fig. 4, one can see that the reconstructed noise not only depends on the sensor noise, but also on the reconstruction algorithm. It is symmetric and has some periodicity and strong similarities for different angles. As a consequence, the features we proposed to extract from the noise image aim at putting in evidence such periodicity and similarity to discriminate the

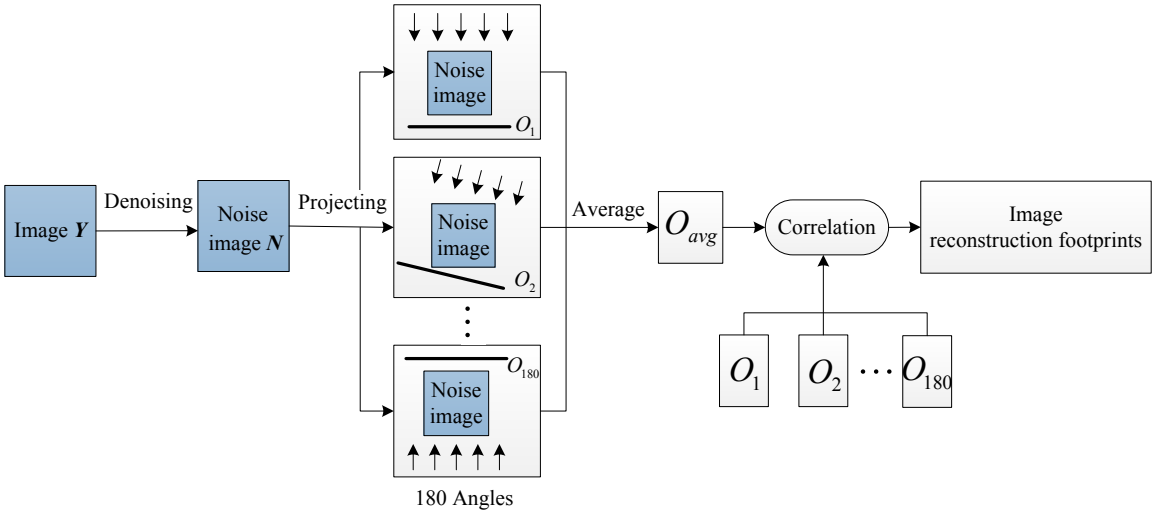

Fig. 6. CT 3D image reconstruction algorithm footprint extraction.

different reconstruction algorithms.

The procedure we propose in order to get these features is illustrated in Fig. 6. For one CT image, its different steps are:

1) Following the steps 1 to 3 of the OSPN extraction procedure to extract the image OSPN O_{avg}.
2) In order to evaluate the noise similarity characteristics attached to a reconstruction algorithm, we compute a set of correlation measures $C(j)$, j = 1, 2, …, k, in-between projection angle noise estimates O_j, j = 1, 2, …, k, and the average angle noise O_{avg}, i.e., the image OSPN.

$$C(j) = corr\left(O_{avg}, O_j\right) = \frac{\left(O_{avg} - \overline{O_{avg}}\right)\cdot\left(O_j - \overline{O_j}\right)}{\left\|O_{avg} - \overline{O_{avg}}\right\|\cdot\left\|O_j - \overline{O_j}\right\|}, j = 1,\cdots \quad (6)$$

where $\overline{O_{avg}}$ and $\overline{O_j}$ are the average of O_{avg} and O_j, respectively. In this work, the value of k is fixed to 180.

These correlation measures help to capture the noise periodicity caused by the image reconstruction process. They are regrouped within a vector C of $1\times k$ components. C constitutes the 3D image reconstruction algorithm footprint. It will be used to discriminate reconstruction algorithms.

Because we miss of technological and processing information from the CT providers, we propose to use this vector of features as input of a classifier. In the sequel, we exploit Support Vector Machine (SVM) classifiers [31]. In order to illustrate the discriminative power of our 3D CT-Scanner reconstruction footprints, let us come back to our simulation framework, where 100 different Gaussian noises n_u, u = 1, 2, …, 100, were generated and used as input of the 5 image reconstruction algorithms presented above, i.e., R_i, i = 1, 2, …, 5, leading thus to 500 reconstructed noisy images I_{Ri}. The respective footprints of these images were then calculated: $C_{Ri}^u, u = 1,\cdots$, $i = 1,\cdots$. We give in Fig. 7, the correlation values we obtained in-between the footprint C_{R2}^1 and the 500 others. As it can be seen the maximum correlation is achieved for C_{R2}^1 and the 100 other footprints C_{R2}^u, $u = 1,\cdots$, i.e., the other 100 simulated noises processed with the same reconstruction algorithm R_2. One can also see that there is a clear gap between the correlations C_{R2}^1 and C_{Ri}^u, $u = 1,2,...,100$, $i = 1, 3, 4, 5$. Similar results are obtained with other reconstruction algorithms. From these simulated experiments, we expect that our 3D image reconstruction algorithm footprint will be able to discriminate CT-Scanner according to their reconstruction algorithm. As we will see in the sequel, this is the case.

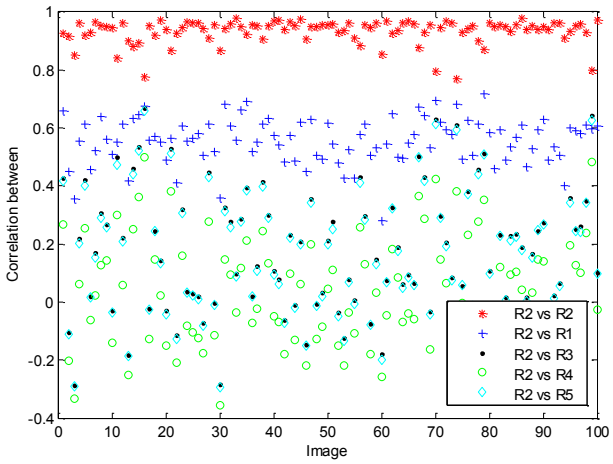

Fig. 7. Correlations between footprints, R_2 *vs.* R_2 is the correlation between C_{R2}^1 and C_{R2}^u, $u = 1,\cdots$; R_2 *vs.* R_i, $i = 1, 3, 4, 5$ corresponds to the correlation between C_{R2}^1 and all other footprints C_{Ri}^u, $u = 1,\cdots$, $i = 1, 3, 4, 5$).

It is important to notice that this experiment also shows that when several CT-Scanners use the same reconstruction algorithm, the proposed footprint will not allow discriminating them. This statement is observable in Fig. 7, where the correlations between the footprint C_{R2}^1 and the other 100 footprints C_{R2}^u, $u = 1,\cdots$, i.e. different CT-Scanners that use the reconstruction algorithm R_2, are always high (see the red crosses). Nevertheless, and as we will see in Section IV. C, when combined with OSPN, our 3D image reconstruction algorithm footprint can reinforce CT scanner identification.

IV. Experiments

We have collected 15 CT image sets from 15 CT-Scanner

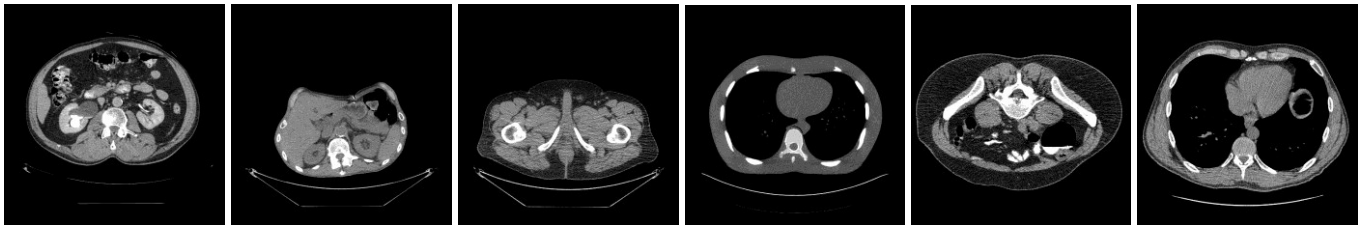

Fig. 8. Illustrate example of our CT image test sets.

TABLE I
LIST OF THE CT-SCANNERS CONSIDERED IN OUR EXPERIMENTS

ID	CT Model	ID	CT Model
A1	GE Bright Speed	B1	Philips Briliance
A2	GE Discovery CT590 RT	B2	Philips Mx8000 IDT
A3	GE Discovery CT750 HD	C1	Siemens Emotion
A4	GE Discovery HR	C2	Siemens Sensation
A5	GE Discovery STE	C3	Siemens Definition
A6	GE Light Speed QXi	D1	Toshiba Aquilion
A7	GE Light Speed	D2	Toshiba Xpeed
A8	GE Light Speed VCT		

models of 4 distinct manufacturers (see Table I) so as to conduct our experiments. Every set is constituted of 200 images of various content (i.e. anatomical objects), leading thus to a global database of 3000 images. Notice that all these images are raw image data (i.e., uncompressed data). We give in Fig. 8 some illustrative samples of our CT image test sets.

In the following, we compare the performance of CT-Scanner identification systems based on the detection of OSPN and SPN into images, respectively. We then present the results we obtained in discriminating CT-Scanner systems based on their reconstruction algorithms. At last, we examine the performance of CT-Scanner identification based on both OSPN and 3D CT-Scanner reconstruction footprint.

A. Comparison OSPN with SPN

In this section, we compare our OSPN based approach with the SPN based approach reported in [26]. Let us recall the principle of these approaches stands on the correlation between the OSPN/SPN of a CT-Scanner, i.e., the reference OSPN/SPN, with the OSPN/SPN extracted from the image under observation. In this experiment, for one CT-Scanner, its reference OSPN or SPN was first extracted using 30 images by averaging their respective OSPN or SPN. Then, 100 other images issued from the same CT-Scanner combined with 1400 other test images of the other CT-Scanners (100 per CT-Scanner) were randomly selected to constitute the test set. The reason why we decided not to use all images in a trial, is to reduce time computation. It also stands on the fact that we observed that the results obtained by randomly selecting 30 reference images and 100 test images are very similar to those obtained with all images. In a trial, images are randomly selected over our whole image set and not from a subset of it.

For all CT-Scanners, Fig. 9 shows the histograms of the

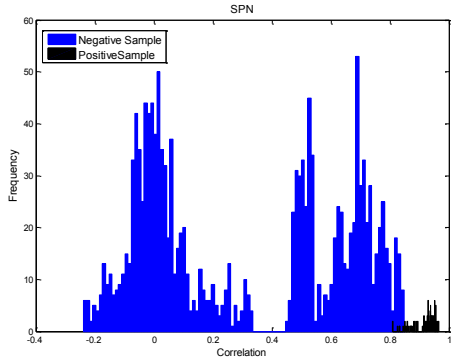

(a)

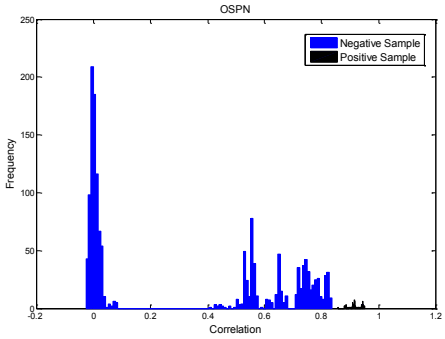

(b)

Fig. 9. (a) Histogram of the SPN correlation values, (b) Histogram of the OSPN correlation values.

correlation values of the SPN and of the OSPN extracted from these images, with the reference SPN and reference OSPN of CT-Scanners. It is observed that correlation values of the positive class (correct identification) and negative class (incorrect identification) cannot be separated clearly with the SPN (Fig. 9(a)), while a clear margin exists between these two classes with the OSPN (Fig. 9(b)).

To go further in this comparison, we use the ROC (Receiver Operating Characteristic) curve, which is obtained by computing the true positive rate (TPR), and the false positive rate (FPR) for a binary classifier system as its discrimination threshold varies, to measure the performance. The respective ROC curves of SPN and OSPN are given in Fig. 10. Again it can be seen that OSPN performs better than SPN.

B. Identification of 3D image reconstruction algorithms

As exposed in section III, this approach stands on the training of an SVM classifier so as to discriminate different CT-Scanners based on their 3D image reconstruction algorithm footprints. Once the classifier built up, this one will take as

TABLE II
CONFUSION CLASSIFICATION RATE MATRIX BASED ON OUR 3D IMAGE RECONSTRUCTION ALGORITHM FOOTPRINTS CONSIDERING THE 15 CT-SCANNERS LISTED IN TABLE 1 AS 15 DISTINCT CLASSES

ID	A1	A2	A3	A4	A5	A6	A7	A8	B1	B2	C1	C2	C3	D1	D2
A1	**96.3**	1.27	0.76	0.27	0	1.4	0	0	0	0	0	0	0	0	0
A2	1.27	**91.6**	1.27	0.6	1.46	1.26	1.27	1.27	0	0	0	0	0	0	0
A3	0.46	1.3	**94.41**	0	0.03	0.9	2.13	0.77	0	0	0	0	0	0	0
A4	0.43	0	0	**99.24**	0	0	0.33	0	0	0	0	0	0	0	0
A5	0	0.5	0	0	**96.16**	0	3.34	0	0	0	0	0	0	0	0
A6	2.37	1.1	1.33	0	0.03	**95.04**	0.13	0	0	0	0	0	0	0	0
A7	0	2.93	2.13	0	3.33	0.13	**84.95**	6.53	0	0	0	0	0	0	0
A8	0	1.27	0.77	0	0	0	6.52	**91.44**	0	0	0	0	0	0	0
B1	0	0	0	0	0	0	0	0	**97.11**	0.67	0.76	0.73	0.73	0	0
B2	0	0	0	0	0	0	0	0	0.53	**95.61**	1	0.6	2.26	0	0
C1	0	0	0	0	0	0	0	0	0.43	0.4	**97.2**	1.27	0.7	0	0
C2	0	0	0	0	0	0	0	0	1.73	0.26	1.43	**95.98**	0.6	0	0
C3	0	0	0	0	0	0	0	0	0.37	1.97	1.37	0.53	**95.76**	0	0
D1	0	0	0	0	0	0	0	0	0	0	0	0	0	**97.78**	2.22
D2	0	0	0	0	0	0	0	0	0	0	0	0	0	2.96	**97.04**

input the footprint of the image we want to find out the origin of. The following results are given in average after having trained our SVM classifier 5 times with different learning CT-Scanner image sets of 30 images randomly selected. At each time, the classifier is by next tested choosing randomly 100 other images. The average confusion matrix of classification rates is given in Table II, where the $(i, j)^{th}$ entry denotes the percentage of images that belong to the i^{th} CT-Scanner (row) and which have been identified as issued from the j^{th} CT-Scanner (column). As it can be seen, the overall classification accuracy is in average of 95.04% with a standard deviation of 3.48%. Herein, our system is able to distinguish CT-Scanners since they use different image reconstruction algorithms. Nevertheless, it is important to recall that if two CT-Scanners use the same reconstruction algorithm; our system will not be able to discriminate them (see last experiments of Section III. B).

C. CT-Scanner identification based on both OSPN and 3D image reconstruction algorithm footprints

Herein, we examine the identification of a CT-Scanner using both OSPN and 3D image reconstruction algorithm footprints. In this experiment, the 3D image reconstruction algorithm footprint vector C is concatenated with OSPN vector, and then used as classifier input. More precisely, the considered image footprint corresponds to a vector whose components are: the image OSPN (512 samples) and 3D image reconstruction algorithm footprint (180 samples). As in the previous experiment, the following results are given in average after 5 trials. At each time our SVM was trained on different learning set containing 30 images and testing set of 1500 other images (100 per scanner) randomly chosen from our whole test set. The average confusion matrix of the classification rates we obtained are given in Table III. As it can be seen, the overall classification accuracy is about 96.65% with a standard deviation of 1.22%. In order to go further in the performance comparison of this last system with the schemes based on SPN or OSPN, respectively, we give in Fig. 10 their respective ROC curves after 5 iterations. Notice that the ROC Curve of our SVM based system has been achieved following the approach

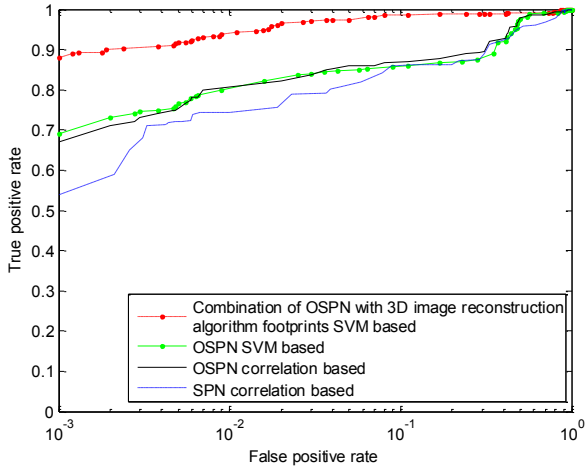

Fig. 10. ROC curves of image origin identification schemes based on: SPN-correlation, OSPN-correlation, OSPN-SVM and the combination of OSPN with 3D image reconstruction algorithm footprints with SVM.

given in [17] by computing the fractions of correctly and wrongly classified images, while making varying parameter values associated to the SVM kernel function. In our experiments, the radial basis function (RBF) was used. Both Fig. 10 and table III show that the hybrid approach provides better results than the approach based only on one set of footprints (OSPN or reconstruction algorithm footprints).

In order to refine the gain of performance of the hybrid approach compared to OSPN, we conducted one last experiment where we trained an SVM using only OSPN as input. The average confusion matrix of the classification rates we obtained, after having trained our SVM classifier as previously (i.e., 5 times with different learning/training CT-Scanner image sets), is given in Table IV. As it can be seen, the overall classification accuracy is in average of 93.84% and is below the performance of the hybrid approach. To complete this experiment, we also give in Fig. 10 the ROC curve obtained with the hybrid approach after 5 iterations (see green curve). It can be seen that it achieves equivalent performance compared to the OSPN correlation based detection results of Section IV. A.

As far as we know, different underlying reasons can

TABLE III
CONFUSION CLASSIFICATION RATE MATRIX OF OUR SCHEME BASED ON BOTH OSPN AND 3D IMAGE RECONSTRUCTION ALGORITHM FOOTPRINTS CONSIDERING 15 CT-SCANNERS LISTED IN TABLE 1 AS 15 CLASSES

ID	A1	A2	A3	A4	A5	A6	A7	A8	B1	B2	C1	C2	C3	D1	D2
A1	**97.56**	0.83	0	0.52	0	1.09	0	0	0	0	0	0	0	0	0
A2	0.67	**95.8**	1.02	0	0	0.57	1.63	0.31	0	0	0	0	0	0	0
A3	0	1.07	**95.11**	0	0	1.16	1.87	0.79	0	0	0	0	0	0	0
A4	1.7	0	0	**98.3**	0	0	0	0	0	0	0	0	0	0	0
A5	0	0	0	0	**96.73**	0	3.27	0	0	0	0	0	0	0	0
A6	1.67	1.1	0.84	0	0	**96.39**	0	0	0	0	0	0	0	0	0
A7	0	1.29	0.43	0	1.21	0	**94.77**	2.3	0	0	0	0	0	0	0
A8	0	0.86	1.04	0	0	0	3.27	**94.83**	0	0	0	0	0	0	0
B1	0	0	0	0	0	0	0	0	**96.1**	1.67	0.76	0.71	0.76	0	0
B2	0	0	0	0	0	0	0	0	0.87	**96.13**	0.81	0.41	1.78	0	0
C1	0	0	0	0	0	0	0	0	0.52	0.27	**96.82**	1.88	0.51	0	0
C2	0	0	0	0	0	0	0	0	0.33	0.16	1.47	**97.08**	0.96	0	0
C3	0	0	0	0	0	0	0	0	0.15	0.86	0.34	1.09	**97.56**	0	0
D1	0	0	0	0	0	0	0	0	0	0	0	0	0	**98.63**	1.37
D2	0	0	0	0	0	0	0	0	0	0	0	0	0	2.01	**97.99**

TABLE IV
CONFUSION CLASSIFICATION RATE MATRIX OF OUR SCHEME BASED ON OSPN ONLY AS INPUT OF A SVM CLASSIFIER CONSIDERING 15 CT-SCANNERS AS 15 CLASSES

ID	A1	A2	A3	A4	A5	A6	A7	A8	B1	B2	C1	C2	C3	D1	D2
A1	**94.27**	1.13	1.23	0.41	0.89	0.45	1.09	0.53	0	0	0	0	0	0	0
A2	0.83	**94.2**	1.12	0.88	0.32	0.96	1.04	0.65	0	0	0	0	0	0	0
A3	0.89	1.04	**93.31**	0.98	0.87	0.66	1.37	0.88	0	0	0	0	0	0	0
A4	0.27	0.88	1.99	**94.39**	1.37	0.41	0.48	0.21	0	0	0	0	0	0	0
A5	0.77	0.16	0.62	1.66	**94.88**	0.31	0.79	0.81	0	0	0	0	0	0	0
A6	0.32	0.79	0.64	0.37	0.13	**92.7**	3.48	1.57	0	0	0	0	0	0	0
A7	0.87	0.99	0.82	0.32	1.01	3.2	**90.62**	2.17	0	0	0	0	0	0	0
A8	0.59	0.41	0.89	0.19	0.87	1.86	2.35	**92.84**	0	0	0	0	0	0	0
B1	0	0	0	0	0	0	0	0	**95.74**	1.71	0.82	0.69	1.04	0	0
B2	0	0	0	0	0	0	0	0	1.84	**94.32**	0.96	0.81	2.07	0	0
C1	0	0	0	0	0	0	0	0	0.52	0.27	**95.17**	1.88	0.51	0	0
C2	0	0	0	0	0	0	0	0	0.47	0.79	1.77	**95.73**	1.24	0	0
C3	0	0	0	0	0	0	0	0	1.61	1.92	1.64	1.51	**93.32**	0	0
D1	0	0	0	0	0	0	0	0	0	0	0	0	0	**93.22**	6.78
D2	0	0	0	0	0	0	0	0	0	0	0	0	0	7.15	**92.85**

contribute to explain misclassifications. They depend on the closeness of the CT scanners in terms of signal processing (e.g. reconstruction algorithms) and electronic components (e.g. X-Ray Tube) and also on the quality or noisiness of the image. The noisier the image, the more difficult is the extraction of the image OSPN and 3D image reconstruction algorithm footprints. However, more experiments with broader image sets are necessary to identify the contribution or influence of these aspects onto the performance of the above approaches.

V. CONCLUSION

In this paper, three approaches have been proposed to identify the CT-Scanner that has issued an image. They take advantages of the principles of CT-Scanner acquisition chain and of the presence of an inherent array sensor noise. We have shown that: i) it is possible to extract the original sensor pattern noise from an image by inverting back the simple back projection algorithm and ii) this OSPN can be used to better discriminate the origin of an image than solutions proposed for general public devices. We also proposed a 3D reconstruction algorithm footprint which put in evidence periodicities and similarities of such algorithms onto OSPN. As experimentally shown, when combined, these sets of features constitute a robust CT-Scanner footprint with very high detection capability. However, in order to generalize our results, further experiments have to be conducted on a broader set of images and devices. Moreover, as the quality of our footprints depends on the image denoising process, future works will focus on identifying the most adapted image filter.

ACKNOWLEDGMENT

Experimental data set have been provided with the courtesy of MEDECOM Company, 9 Bis Rue de Kerbrat, 29470 Plougastel-Daoulas, FRANCE.

REFERENCES

[1] W. Pan, G. Coatrieux, D. Bouslimi, *et al.* "Secure public cloud platform for medical images sharing," *Studies in health technology and informatics*, pp. 251-255, 2014.

[2] W. Pan, G. Coatrieux, N. Cuppens-Boulahia, *et al*. "Medical Image Integrity Control Combining Digital Signature and Lossless Watermarking," *in Lecture Notes in Computer Science Volume 5939,* pp. 153-162, 2010.

[3] W.D. Bidgood, S.C. Horii, F.W. Prior, *et al.* "Understanding and using DICOM, the data interchange standard for biomedical imaging," *J. American Medical Informatics Association*, vol. 4, no. 3, pp. 199-212, 1997.

[4] G. Coatrieux, H. Huang, H.Z. Shu, *et al.* "A watermarking based medical image integrity control system and an image moment signature for tampering characterization," *IEEE journal of biomedical and health informatics,* vol. 17, pp. 1057-1067, 2013.
[5] S. Alam, A. Jamil, A. Saldhi, *et al.* "Digital image authentication and encryption using digital signature," *IEEE International Conference on Advances in Computer Engineering and Applications (ICACEA),* pp. 332-336, 2015.
[6] D.S. Prathiwi, W. Astuti, Adiwijaya, *et al.* "Watermarking scheme for authenticity and integrity control of digital medical image using Reed-Muller Codes and Hash Block Chaining," *International Conference on Information and Communication Technology (ICoICT),* pp. 23-29, 2015.
[7] J. Ouyang, G. Coatrieux, H.Z. Shu, "Robust hashing for image authentication using quaternion discrete Fourier transform and log-polar transform," *Digital Signal Processing*, pp. 98-109, 2015.
[8] W. Pan, G. Coatrieux, J. Montagner, *et al.* "Comparison of some reversible watermarking methods in application to medical images," *IEEE International Conference of the Engineering in Medicine and Biology Society, EMBC*, pp. 2172-2175, 2009.
[9] D. Bouslimi, G. Coatrieux, C. Quantin, *et al.* "A Teleassistance Protocol Based on Joint Watermarking-Encryption Evidence for Identification of Liabilities in Case of Litigation," *Innovation and Research in BioMedical Engineering (IRBM),* vol. 36, no 5, pp. 279-286, 2015.
[10] G. Coatrieux, H. Huang, H.Z. Shu, *et al.* "A watermarking-based medical image integrity control system and an image moment signature for tampering characterization," *IEEE Journal of Biomedical and Health Informatics*, vol. 17, no. 6, pp. 1057-1067, 2013.
[11] M.C. Stamm, M. Wu, K.J.R. Liu, "Information forensics: An overview of the first decade," *IEEE, Access,* vol. 1, pp. 167-200, 2013.
[12] H.T. Sencar, N. Memon. "Digital image forensics," 2013.
[13] S. Bayram, H. Sencar, N. Memon, *et al.* "Source camera identification based on CFA interpolation," *IEEE International Conference on Image Processing, ICIP,* pp. 69-72, 2005.
[14] A. Swaminathan, M. Wu, K.J.R. Liu, "Nonintrusive component forensics of visual sensors using output images," *IEEE Transactions on Information Forensics and Security,* vol. 2, no. 1, pp. 91-106, 2007.
[15] Z. Deng, A. Gijsenij, J. Zhang, "Source camera identification using auto-white balance approximation," *IEEE International Conference on Computer Vision, (ICCV),* pp. 57-64, 2011.
[16] C.K. San, E.Y. Lam, K.K.Y. Wong, "Source camera identification by JPEG compression statistics for image forensics," *IEEE Region 10 Conference TENCON 2006,* pp. 1-4, 2006.
[17] H. Gou, A. Swaminathan, M. Wu, "Intrinsic sensor noise features for forensic analysis on scanners and scanned images," *IEEE Transactions on Information Forensics and Security,* vol. 4, no. 3, pp. 476-491, 2009.
[18] S. Lyu, "Natural Image Statistics in Digital Image Forensics," *Springer New York,* 2013.
[19] G. Gerules, S.K. Bhatia, D.E. Jackson, "A survey of image processing techniques and statistics for ballistic specimens in forensic science," *Science & Justice,* vol. 53, no. 2, pp. 236-250, 2013.
[20] C.K. San, E.Y. Lam, K.K.Y. Wong. "Automatic source camera identification using the intrinsic lens radial distortion," *Optics Express,* vol. 14, no. 24, pp. 11551-11565, 2006.
[21] J. Lukas, J. Fridrich, M. Goljan. "Determining digital image origin using sensor imperfections," *Electronic Imaging 2005. International Society for Optics and Photonics,* pp. 249-260, 2005.
[22] T. Thai, R. Cogranne, F. Retraint. "Camera model identification based on the heteroscedastic noise model," *IEEE Transactions on Image Processing,* vol. 23, pp. 250-263, 2014.
[23] J. Lukas, J. Fridrich, M. Goljan, "Digital camera identification from sensor pattern noise," *IEEE Transactions on Information Forensics and Security*, vol. 1, pp. 205-214, 2006.
[24] M. Chen, J. Fridrich, M. Goljan, *et al.* "Source digital camcorder identification using sensor photo response non-uniformity," *Electronic Imaging 2007. International Society for Optics and Photonics,* pp. 65051G-65051G-12, 2007.
[25] Y. Duan, G. Coatrieux, H.Z. Shu. "Identification of digital radiography image source based on digital radiography pattern noise recognition," *IEEE International Conference on Image Processing, ICIP,* pp. 5372-5376, 2014.
[26] A. Kharboutly, W. Puech, G. Subsol, *et al*. "CT-Scanner identification based on sensor noise analysis," *IEEE 5th European Workshop on Visual Information Processing, EUVIP,* pp. 1-5, 2014.
[27] E. Seeram. "Computed tomography: physical principles, clinical applications, and quality control," *Elsevier Health Sciences,* 2013.
[28] R. Cierniak, "X-ray computed tomography in biomedical engineering," *Springer,* 2011
[29] M. Beister, D. Kolditz, W.A. Kalender, "Iterative reconstruction methods in X-ray CT," *Physica Medica,* vol. 28, pp. 94-108, 2012.
[30] J. Hsieh, B. Nett, Z. Yu, *et al.* "Recent advances in CT image reconstrution," *Current Radiology Report*, pp. 39-51, 2013.
[31] U.H.G. Kressel, "Pairwise classification and support vector machines," *Advances in kernel methods*, pp. 255–268, 1999.

Yuping Duan received the B.S. and the M.S. degree in electrical and information engineering, from Anhui University of Science and Technology, in 2008 and 2011 respectively. Since September 2011, she has been working toward the Ph.D. degree in biomedical engineering, from Southeast University, Nanjing, China; and in Institut Mines-Telecom, from Telecom Bretagne, Brest, France. Her research interest includes medical information system security, and medical image processing.

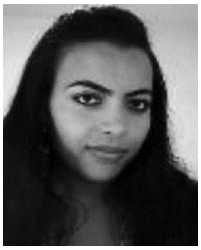

Dalel Bouslimi (M'12) received the Ph.D. Degree from Telecom Bretagne in December 2013 after the Engineering Degree in computer science and the Master's degree in image from the Ecole Nationale des Sciences de l'Informatique, Manouba, Tunisia, in 2009 and 2010, respectively. Since January 2014, she is a Postdoctoral Researcher with the Department of Information and Image Processing, Tele com Bretagne, conducting her research activities in the Laboratory of Medical Information processing (LaTIM Inserm UMR 1101) and in the Joint Laboratory on Security and Processing of Externalized Medical Image Data (SePEMeD). Her main areas of research interest are digital content forensics, processing of encrypted data and medical data protection by means of watermarking and encryption.

Guanyu Yang received the B.S. degree and M.S. degree in biomedical engineering from Southeast University, Nanjing, China in 2002 and 2005 respectively, Ph.D. degree in signal and image processing from University of Rennes, Rennes, France, in 2009. He is an associated professor in the School of Computer Science and Engineering in Southeast University, Nanjing, China. His research interests are mainly focused on medical image processing, computer-assisted systems for diagnosis and therapy in medicine.

Huazhong Shu (SM'06) received the B.S. degree in applied mathematics from Wuhan University, China, in 1987, and the Ph.D. degree in numerical analysis from the University of Rennes, France, in 1992. He is now a professor with the Department of Computer Science and Engineering of Southeast University, China. His recent work concentrates on the image analysis, pattern recognition, and fast algorithms of digital signal processing.

Gouenou Coatrieux (SM'13) received the Ph.D. degree in signal processing and telecommunication from the University of Rennes I, Rennes, France, in collaboration with the Ecole Nationale Supérieure des Télécommunications, Paris, France, in 2002. He is currently a professor with the Information and Image Processing Department, Institut Mines-Telecom, Telecom Bretagne, Brest, France. His research is conducted in the LaTIM Laboratory, INSERM U1101, Brest. His primary research interests concern medical information system

security, watermarking, crypto-watermarking, secure processing of outsourced data, digital forensics in medical imaging, electronic patient records.